Heliyon 10 (2024) e27757

Contents lists available at ScienceDirect

Heliyon

journal homepage: www.cell.com/heliyon

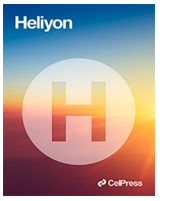

Research article

# Colorimetric and fluorescent dual-biosensor based on zirconium and preasodium metal-organic framework (zr/pr MOF) for miRNA-191 detection

Mahsa Dehnoei [a], Elnaz Ahmadi-Sangachin [a], Morteza Hosseini [a,b,*]

[a] *Nanobiosensors lab, Department of Life Science Engineering, Faculty of New Sciences & Technologies, University of Tehran, Tehran 1439817435, Iran*

[b] *Department of Pharmaceutical Biomaterials, Medical Biomaterials Research Center, Faculty of Pharmacy, Tehran University of Medical Sciences, Tehran, Iran*

A B S T R A C T

MicroRNAs (miRNAs) are associated with certain types of cancer, tumor stages, and responses to treatment, thus efficient methods are required to identify them quickly and accurately. Abnormal expression of microRNA-191 (miR-191) has been linked to particular cancers and several other health conditions, such as diabetes and Alzheimer's disease. In this study, a new dual-biosensor based on the zirconium and preasodium-based metal-organic framework (Zr/Pr MOF) was developed for the rapid, ultrasensitive, and selective detection of miRNA-191. The synthesized Zr/Pr MOF exhibited peroxidase-like activity and fluorescence properties. Our dual method involves monitoring the fluorescence and peroxidase activity of metal-organic frameworks (MOFs) in the presence of miRNAs. The Zr/Pr MOF can catalyze hydrogen peroxide ($H_2O_2$) to oxidize the chromogenic substrate 3, 3′, 5, 5′-tetramethylbenzidine (TMB) to produce blue oxidized TMB (oxTMB), which exhibits ultraviolet absorption at 660 nm. However, the addition of a label-free miRNA-191 probe caused a significant change in fluorescence intensity and absorbance, indicating the binding of single-stranded miRNAs to the MOF through van der Waals interactions and π-π stacking. The presence of the target miRNA-191 caused the probe to be released from the surface of the MOF owing to hybridization, which increased the peroxidase-like activity of Zr/Pr-MOF. Both response signals showed acceptable linear relationship and low detection limits. Fluorescence and colorimetry have an LOD of 0.69 and 8.62 pM, respectively. This study demonstrates the reliability and sensitivity of miRNA identification in human serum samples.

## 1. Introduction

Research has demonstrated that small, noncoding microRNAs (miRNAs) may play a significant role in the development of diseases such as cancer [1]. Studies have indicated that both increases and decreases in the activity of miRNAs can lead to the formation of cancer through various pathways [2,3]. Additionally, miRNA expression is linked to certain types of cancer, tumor stage, and response to treatment [4]. Therefore, there is a need to develop new and efficient methods for rapid and accurate identification of miRNAs in cells, tissues, and fluids, such as serum and plasma [5]. In particular, miR-191 is abnormally expressed in more than twenty different types of cancer [6], including acute myeloid leukemia [7], female [8] and male [9] breast cancer, prostate cancer [10], colorectal cancer [11], lung cancer [12], and osteosarcoma [13]. In addition, altered expression of miR-191 has been linked to a number of other health conditions, such as type-2 diabetes [14], Alzheimer's disease [15], and idiopathic nephrotic syndrome [16]. In conclusion, developing methods to accurately and safely measure miR-191 levels in patients could help fight these underlying diseases [6].

* Corresponding author. Nanobiosensors lab, Department of Life Science Engineering, Faculty of New Sciences & Technologies, University of Tehran, Tehran 1439817435, Iran.

*E-mail address:* hosseini_m@ut.ac.ir (M. Hosseini).

https://doi.org/10.1016/j.heliyon.2024.e27757

Received 16 December 2023; Received in revised form 6 March 2024; Accepted 6 March 2024

Available online 14 March 2024

The use of conventional methods, such as northern blotting and reverse transcription-polymerase chain reaction (qRT-PCR), for the detection of miRNAs has been widely adopted because of their diagnostic value. These methods, however, are not very sensitive and require laborious, complicated, and time-consuming procedures that are challenging to include in standard miRNA analysis. As a result, it is essential to create efficient and cost-effective miRNA detection techniques [17].

Currently, a number of nanostructured materials, including carbon nanotubes [18], graphene oxide, gold nanoparticles [19], and metal-organic frameworks (MOFs) [20], have been exploited as novel tools for constructing nucleic acid-based biosensors. Metal-organic framework-based biosensors provide a number of benefits over other materials, including a larger loading capacity, conjugated π-electron systems [21], tunable porosity [22], enhanced surface area [23], and lower fabrication costs [24]. The efficacy of these biosensors is highly dependent on the detection methods employed, such as electrochemical (EC) [25], electrochemiluminescence (ECL) [26], fluorescence (FL) [27], and colorimetry [28]. Fluorescence-based detection assays and colorimetric techniques have been employed to develop a simple, extremely sensitive approaches with distinct color variation [29] that does not require expensive equipment [30]. The fluorescence of MOFs can eliminate the need for additional fluorescent probes, simplify the experimental procedure, reduce the cost of the experiment, and increase detection precision [31].

Through the selection of suitable metal ions and ligands, one can precisely tailor the properties of MOFs [32]. Mixed-metal MOFs, comprising of a blend of metal ions and organic ligands, provide several advantages over single-metal MOFs. Introducing bimetallic centers into the same MOF framework has the potential to create defects and a notable synergistic effect among metal sites. This could increase the number of active sites, thereby enhancing electrochemical performance [33].

By manipulating the ratio and types of metal ions and organic ligands, MOFs can be designed to have adjustable enzyme-like activity and fluorescence properties. The fabrication of MOFs with intrinsic properties is more practical and valuable for many applications, given the stability of the MOFs and the use of low-cost precursors [34,35].

UiO-66, composed of Zr6 clusters and terephthalic acid, can load DNA molecules [36]. Zr-based MOFs have been demonstrated to have a strong affinity for phosphate groups in biomolecules and towards double- and single-stranded DNA [37].

Recent studies have shown the potential of MOFs to precisely capture and release small molecules [38]. A recent study demonstrated that MOFs can be used for the precise capture and release of single-stranded nucleic acids. This suggests that MOFs can potentially be used to detect miRNAs via RNA-RNA hybridization [39]. Recent research has demonstrated that the π-π stacking effect, static and coordinative interactions between the basic group and the aromatic rings of the material, and the phosphate group and metal ions all contribute to the absorption of miRNA on material surfaces. This method is highly effective for biosensor analysis [40].

In this study, we have developed a dual biosensor based on a zinc and praseodymium metal-organic framework (Zr/Pr MOF) for the rapid, ultrasensitive, and selective detection of microRNA (miRNA) molecules. The bimetal MOF was synthesized using a

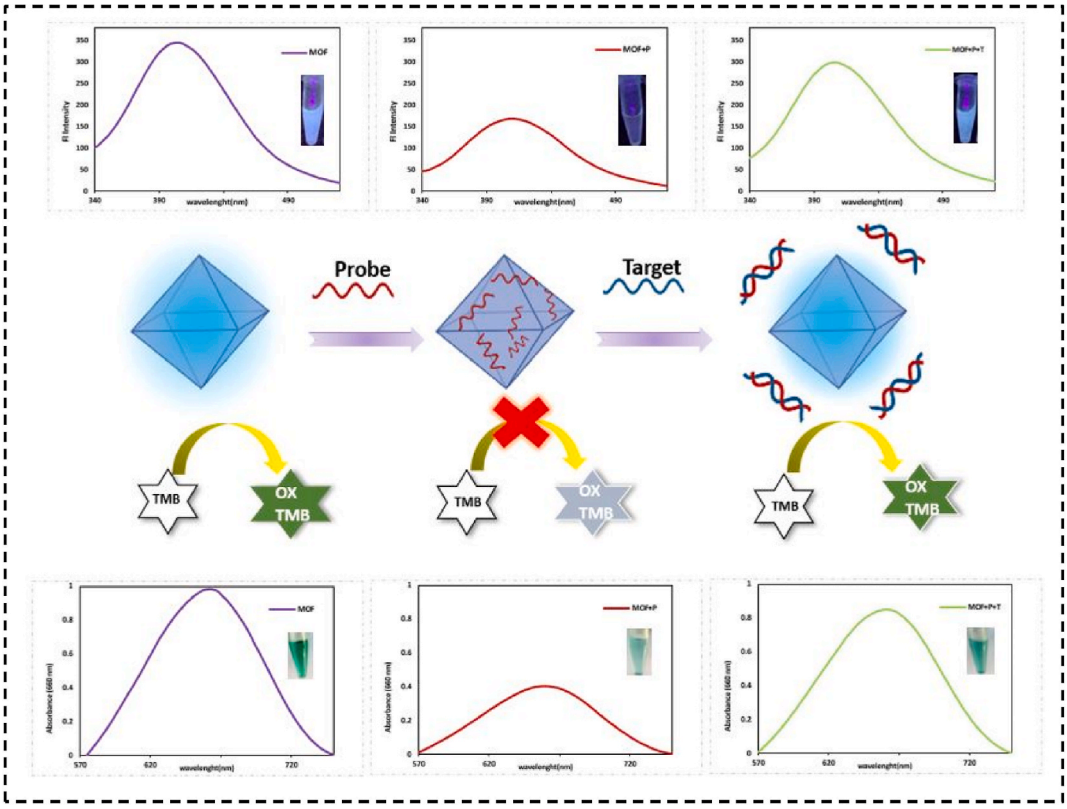


**Fig. 1.** Schematic diagram of colorimetry and fluorescence dual-mode detection miRNA-191.

hydrothermal method [41] and was found to exhibit both fluorescent and colorimetric properties when exposed to substrates such as TMB and $H_2O_2$. The addition of a label-free miRNA-191 probe caused a significant change in fluorescence intensity and absorbance, indicating the binding of single-stranded miRNAs to the Zr/Pr MOF through van der Waals interactions and π-π stacking. When a target miRNA strand was added, the resulting hybridization led to an increase in both fluorescence intensity and UV absorbance (Fig. 1). Hence, for the first time, a dual-mode detection method for miRNA that relies on colorimetric and fluorescence modes has been developed utilizing metal-organic frameworks (MOFs) without the need for fluorescently labeled single-stranded DNA (ssDNA).

## 2. Experimental section

### 2.1. Reagents and instruments

#### 2.1.1. Materials

Zirconium (IV) oxynitrate hydrate (Zr), praseodymium (Pr), 1,4-benzene-dicarboxylic acid ($H_2BDC$), N, N-di-methyl formamide (DMF), 3,3′,5,5′-tetramethylbenzidine (TMB), dimethyl sulfoxide (DMSO), hydrogen peroxide ($H_2O_2$), Tris-EDTA, HCl (for preparing TE buffer), Sodium Phosphate Dibasic Heptahydrate, Sodium Phosphate Monobasic Monohydrate (for preparing PB buffer), Sodium Acetate, Acetic Acid (for preparing Acetate Buffer) were purchased from Merck Millipore and Sigma-Aldrich (USA). All materials were of analytical reagent grade, and deionized water with 18.2 MΩ resistivity was obtained from a Millipore Milli-Q system. Human serum samples were provided by Milad Hospital, and all synthetic oligonucleotide sequences included in Table S1 were acquired from Metabion International AG (Planegg, Germany).

#### 2.1.2. Apparatus

The visible light spectrum was studied using a PerkinElmer Lambda 25 UV–Vis spectrometer in the range 200–800 nm. Scanning electron microscopy (SEM) images were obtained using an XL30 ESEM FEG scanning electron microscope. X-ray powder diffraction (XRD) spectroscopy was performed using a Philips diffractometer. A Fourier transform infrared (FT-IR) spectrometer (Shimadzu 8400S) was used to record the FTIR spectra. The fluorescence spectra were measured using an LS-55 fluorometer (PerkinElmer) in the wavelength range of 280–600 nm. Energy dispersive X-ray spectroscopy (EDX) was conducted with a Tescan model energy dispersive spectrometer, and for the measurement of zeta-potential, a Zetasizer Nano-Z (Malvern Instruments, UK) was applied.

### 2.2. Preparation of materials

#### 2.2.1. Zr/Pr-MOF

Zr/Pr-MOF was synthesized using a procedure that has previously been reported [41]. Briefly, in this experiment, $H_2BDC$ (127.6 mg) and DMF (3.6 mL), Zirconium (IV) oxynitrate hydrate (0.533 M, 99.0 mg, 0.800 mL water), and formic acid 100% (1.03 ml) were added to an aqueous solution of Pr (0.533 M, 117 mg, 0.400 mL water), followed by three steps. The mixture was stirred at 100 °C for 15 min while being heated, centrifuged, washed, and the obtained white solid was dried.

#### 2.2.2. Preparing Probe/MOF

The preparation of the probe-MOF included the following steps: 10 μL of the probe miRNA-191 (100 M) was diluted in 10 μl of PB buffer (10 mM, pH = 5), which had previously been dissolved in TE buffer (100 M, pH = 7). The solution was then mixed with 10 μL of target miRNA-191 solutions of varying concentrations. The resulting solutions were heated to 85 °C for 5 min to denature them. The temperature was then gradually reduced until it reached room temperature. After the addition of 40 μL of 2.3 mg/mL MOF dispersed in deionized water, the above-mentioned solutions were incubated for 60 min at room temperature.

#### 2.2.3. Peroxidase-like activity of Zr/Pr-MOF

In PB buffer (10 mM, pH = 5), TMB and $H_2O_2$ were used to test the Zr/Pr MOF's peroxidase-like activity. After 10 min of incubation at predetermined intervals, TMB (50 μl, 10 mM) and $H_2O_2$ (50 μl, 10 mM) were added to 50 μl of Zr/Pr-MOF solution. The UV–Vis absorption was then measured using a standard quartz cell.

## 3. Results and discussions

### 3.1. Characterizations of Zr/Pr-MOF

The SEM images of the prepared Zr/Pr MOFs revealed a spherical morphology, which is in agreement with previous studies (fig. S2A) [42]. In figure (S2.B), the XRD pattern of UiO-66 MOF was presented, with 2θ of 11.84°, 17.19°, 18.74°, 25.39°, and 29.94° indicating the crystalline structure of the MOFs [43]. The EDX spectrum clearly indicated the presence of C, O, Zr, and Pr in the Zr/Pr-MOF structure (fig. S2C). The FT-IR spectrum of the Zr/Pr-MOFs is shown in fig (S2D) and exhibited three peaks related to the C═C bond in the benzene ring of $H_2BDC$ at 1573 $cm^{-1}$, 1403 $cm^{-1}$, and 1358 $cm^{-1}$. The MOF carboxyl groups were stretched symmetrically and asymmetrically, as indicated by the peaks at 1256 cm-1 and 1102 $cm^{-1}$. The peak at 779 $cm^{-1}$, the ligand was visible, and the peak at 480 cm-1 was attributed to Zr–*O*–Zr vibrations, while the absorption peak at 656 cm-1 was related to the covalent link between Pr and oxygen (Pr–O) [35,36].

### 3.2. Fluorescence of Zr/Pr MOF

The fluorescence spectra of $Zr^{+4}$ solution, Pr solution, $H_2BDC$ solution, and Zr/Pr-MOFs were recorded to analyze the fluorescence performance of Zr/Pr-MOFs. As shown in (fig. S3), $H_2BDC$ exhibited a prominent fluorescence peak centered at 380 nm with an excitation wavelength of 290 nm, whereas Zr/Pr-MOFs displayed a fluorescence signal at 406 nm. However, the $Zr^{+4}$ and Pr solutions did not show any detectable fluorescence emission despite undergoing fluorescence analysis. The redshift phenomenon can be explained by Coordination-Induced Emission (CIE),which originates from the forming process of MOFs by $H_2BDC$ and metal ions, leading to a red-shifted emission [44,45]. On the other hand, the binding of the ligand with metals in the MOF structure has led to an increase in emitted fluorescence. The introduction of the ligand into the MOF, considering our ligand-metal ratio, could potentially enhance the stiffness of the ligand within the crystal structure of the MOF. A higher degree of rigidity in the MOF results in reduced energy loss from photo-excitation as heat, ultimately improving radiation relaxation [46].

The fluorescence spectra of the Zr/Pr MOFs and the Zr/Pr MOFs incubated with ssDNA (MOF-P) with and without target miRNA-191 (MOF-P + T) were recorded to analyze the fluorescence performance of the Zr/Pr MOFs. As shown in (Fig. 2A), the Zr/Pr MOFs exhibited outstanding fluorescence emission at 406 nm with an excitation wavelength of 290 nm. The intrinsic fluorescence signal of Zr/Pr MOFs decreased dramatically following the addition of ssDNA (P) to the MOF solution. However, when the target was added, strong fluorescence emission was regained owing to hybridization. Taking advantage of the particular physical and chemical features of adjustable MOF structures, the method of comprehending this fluorescence mechanism is simple, as MOFs with special structures can adsorb ssDNA-label-free probes through electrostatic, π-π stacking, and hydrogen bonding interactions. When these probes come into contact with the MOF surface, fluorescence emission decreases.

This was due to the FRET mechanism. Förster's resonance energy transfer (FRET), also known as fluorescence resonance energy transfer, involves the transfer of energy between a donor fluorophore and an acceptor quencher. In this work, FRET occurred when the energy from the excited Zr/Pr MOF was transferred to the ssDNA, leading to the quenching of the Zr/Pr MOF fluorescence emission. This process provides a simple understanding of the fluorescence mechanism and is a promising method for miRNA detection [47]. Over time, the fluorescence recovery of the MOF-P + T complex occurs due to the competitive hybridization between the complementary target and MOF + P. As a result, ssDNA is released from the MOF surface, leading to the formation of a double-stranded miRNA and ultimately causing the recovery of fluorescence.

### 3.3. Peroxidase-like activity of Zr/Pr-MOF

Today, research into MOFs (metal-organic frameworks) has been used to discover their potential as enzyme mimics due to the presence of organic ligands and metal nodes in their structures [48]. As shown in Fig. 2B, the Zr/Pr-MOFs synthesized in this study displayed remarkable peroxidase-mimicking activity, with a distinct UV–Vis peak at ~660 nm. A colorless to green-blue reaction was observed when $H_2O_2$ and TMB (3, 3′, 5, 5′-tetramethylbenzidine) were added to the MOFs, corresponding to the aforementioned UV–Vis peak. It has been established that the organic linker of Zr/Pr-MOFs is critical for inducing catalytic reactions [41], which was demonstrated through the dipyridyl-based ligands of Zr/Pr-MOFs that serve as mediators to transfer electrons from TMB to $H_2O_2$ (fig. S4).

The presence of the probe caused an observable change in absorbance, indicating the binding of single-stranded (ssDNA) to the Zr/Pr-MOFs through van der Waals interactions and π–π stacking. UV–visible spectroscopy was used to show ssDNA attachment to the Zr/Pr-MOFs. Adding the target led to an increased green-blue color and UV absorbance due to complementary hybridization with the probe, causing the release of the ssDNA probe from the MOFs and the formation of double-stranded structures, resulting in an increase in peroxidase activity. Zeta potential measurements were performed to verify the binding of the miRNA probe to Zr/Pr-MOFs. With

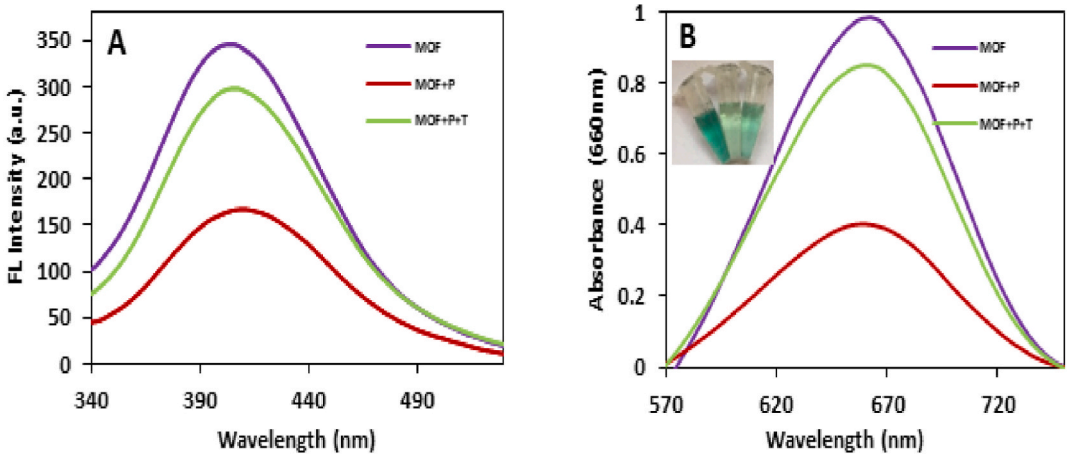


**Fig. 2.** (A) Fluorescence spectra and (B) UV–vis spectra of different systems.

deionized water, a positive zeta potential of +3.99 mV was observed for the Zr/Pr MOFs, indicating its positive charge. After attachment to the ssDNA, the zeta potential was reduced to −12.3 mV, which revealed the binding of the miRNA (fig. S5).

### 3.4. Optimization of assay conditions

The effects of time, buffer, and pH on the fluorescence and absorbance signals were investigated to produce superior detection outcomes. Time-dependent changes in the emission spectrum of the fluorescent MOFs in the presence or absence of a target are shown in fig. S6. Within 60 min, the fluorescence recovery signal of the probe-MOF emission was decreased, suggesting that the incubation procedure was a fast one. (fig. S6A). The fluorescence recovery signal increased with longer hybridization times when miRNA-191 was present, before remaining almost unchanged after 60 min (fig. S6B). These findings led to the selection of 60 min as the ideal incubation time.

Studies have been conducted on how buffers affect emission and absorption signals. As salt may have an impact on the MOF surface charge [49], four buffers including Tris-HCl, PB, PBS, and acetate were added to the MOFs that had been dispersed in deionized water for this purpose. Fluorescence and absorbance were enhanced in the Pb buffer solution, as shown in fig. S7. Next, we examined the effect of pH on the peroxidase-like activity and fluorescence intensity (fig. S8). The maximum peroxidase-like activity occurred at pH = 5, after which the peroxidase-like activity dramatically decreased. The difference in the fluorescent signal (F/F0) reached its maximum at this pH. Therefore, a pH of 5 was determined to be optimal.

### 3.5. Analytical characteristic

Under optimal conditions, a dual strategy of fluorescence and colorimetry was used to measure various concentrations of miRNA-191. As shown in Fig. 3. A The fluorescence intensity of the label-free probe-MOF complex increased with the addition of miRNA-191 in a concentration-dependent manner, which was mainly due to the hybridization of the miRNA target with the probe. Fig. 3. B shows the linear relationship between the concentration of the target miRNA and fluorescence intensity in the ranges of 0.001–100 nM ($R^2$ = 0.9956). According to 3.3 × Sb/m, the limit of detection (LOD) was calculated to be 0.69 pM. Fig. 3C and D illustrate the effectiveness of the colorimetry strategy for detecting miRNA-191. As shown in Fig. 3D–a strong linear relationship was observed between the absorbance rate and the concentration of miRNA-191, from 0.001 to 100 nM ($R^2$ = 0.982). The detection limit was established at 8.62

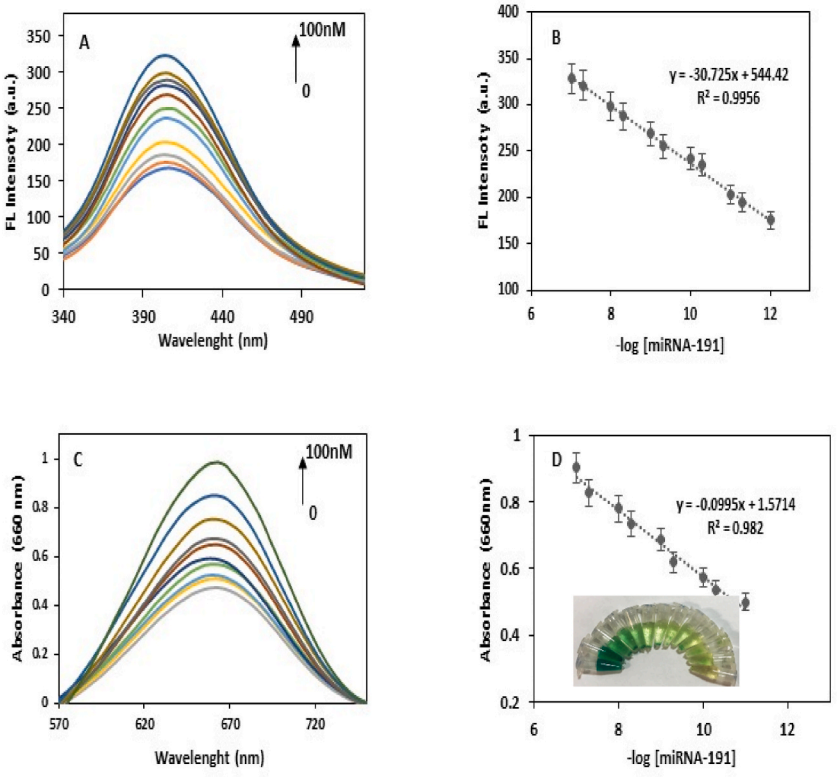


**Fig. 3.** (A) fluorescence spectra with different miRNA-191 concentrations, (B) Linear calibration curves of fluorescence with different miRNA-191 concentrations, (C) UV–vis spectra with different miRNA-191 concentrations, (D) Linear calibration curves of absorbance with different miRNA-191 concentrations.

pM.

### 3.6. Selectivity and stability

To validate the selectivity of the proposed strategy for miRNA-191 detection, several interferences, such as miRNA-103, miRNA-141, miRNA-21, miRNA-155, and a mixture of miRNAs with and without the target, were tested under optimal conditions. Fig. 4A shows that the fluorescence recovery of the detection system significantly increased in the presence of miRNA-191 and the mixture solution containing the target, whereas the other sequences resulted in negligible fluorescence responses. The results demonstrated that none of these non-complementary sequences were able to bind to the particular probe, and no extreme dark green-blue color or increase in absorbance was observed, whereas only the target and its mixture enhanced the color and absorption (Fig. 4B). Our fluorescence method for miRNA detection has a superior linear range and LOD compared to previous MOF-based biosensors, with the exception of electrochemical-based methods, which require complex experimental procedures. The stability of Zr/Pr-MOFs was examined by testing its peroxidase-like activity and fluorescence intensity every five days over the course of a month. The results in fig. S9 show that the peroxidase-like activity and fluorescence properties remained virtually unchanged for the duration of the experiment, indicating that Zr/Pr-MOF displays exceptional stability at room temperature.

The presented technique's ability to detect miRNAs was evaluated and compared to previously reported methods based on sensitivity and linear range assessments, as shown in Table 1. While certain studies have reported lower limits of detection, the proposed method offers several advantages, such as rapid, simple, selective, and dependable detection of miRNAs. These benefits are due to the lack of amplification steps, fluorescence dyes, and enzymatic processes necessary for detection.

### 3.7. Serum sample applications

Several concentrations of miRNA-191 (0.1 nM, 0.5 nM, 1 nM, 2 nM, 5 nM, and 10 nM) were spiked in diluted normal human serum and examined using this dual method under ideal circumstances to evaluate the viability of real samples. The results, presented in Table S2, show satisfactory spiked recoveries in the linear range for both strategies. The fluorescence strategy showed a recovery of 98.5–102.4% with a relative standard deviation (RSD) ranging from 2.07% to 4.3%. And the colorimetry strategy yielded a recovery of 98–102% with an RSD ranging from 2% to 3%. Both techniques had linear ranges with acceptable spike recoveries.

## 4. Conclusion

In summary, a bimetallic Zr/Pr MOF with fluorescent and peroxidase-like properties was used to detect miRNA. The MOF catalyzes the oxidation of the peroxidase substrate TMB to blue oxTMB. The label-free miRNA probe caused a significant change in the fluorescence intensity and absorbance owing to the binding of single-stranded miRNAs to the MOF through van der Waals interactions and π–π stacking. The presence of the target miRNA caused the probe miRNA to be released from the MOF surface owing to hybridization, which increased the peroxidase-like activity of the Zr/Pr-MOF. This strategy is based on changes in the fluorescence and colorimetric properties of the Zr/Pr MOF in the presence of single- and double-stranded RNA. This process is cost-effective, simple, and fast because of its enzyme-free and fluorescent-labeled nature, making it a promising tool for biosensing and medical detection.

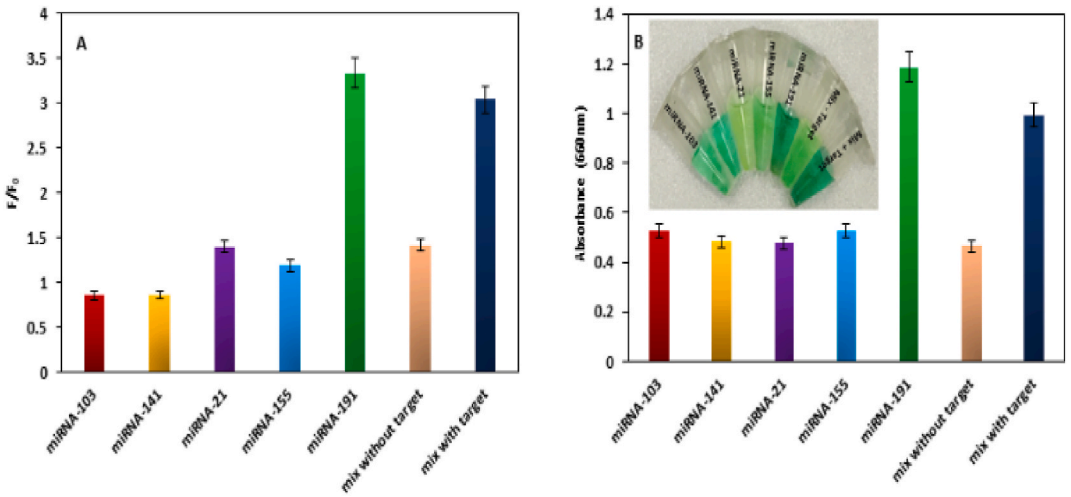


**Fig. 4.** Selectivity of the designed biosensor miRNA-191 on (A) Fluorescence intensity and (B) Absorbance.

**Table 1**
Comparison between this method and other reported methods.

| Targets | Method | Linear range | LOD | References |
|---|---|---|---|---|
| miRNA155 | Electrochemical | 1.00 fM–10 nM | 0.32 fM | [50] |
| miRNA-21, miRNA-96, miRNA-125 | Fluorescence | 0–1000 nM | 10 nM | [51] |
| miRNA-21 | Electrochemical | 1 fM–100 pM | 0.32 fM | [52] |
| miRNA-141 | Electrochemiluminescence | 1 fM–10 pM | 0.30 fM | [53] |
| miRNA21 | Fluorescence | 0–80 nM | 120 pM | [54] |
| miRNA-191 | Fluorescence | 2 pM–200 nM | 0.69 pM | This work |
| miRNA-191 | Colorimetric | 2 pM–200 nM | 8.62 pM | This work |

## Compliance with ethical standards

The authors declare that they have no competing interests.

## CRediT authorship contribution statement

**Mahsa Dehnoei:** Writing – original draft, Methodology, Formal analysis. **Elnaz Ahmadi-Sangachin:** Writing – review & editing, Validation, Methodology, Investigation. **Morteza Hosseini:** Writing – review & editing, Validation, Supervision, Resources, Project administration, Data curation, Conceptualization.

## Declaration of competing interest

The authors declare the following financial interests/personal relationships which may be considered as potential competing interests:Morteza Hosseini reports was provided by University of Tehran. Morteza Hosseini reports a relationship with University of Tehran that includes: employment. The author and the author are faculty members and students of Tehran University. If there are other authors, they declare that they have no known competing financial interests or personal relationships that could have appeared to influence the work reported in this paper.

## Acknowledgments

Financial assistance for this work was provided by Tehran University (No).

## Appendix A. Supplementary data

Supplementary data to this article can be found online at https://doi.org/10.1016/j.heliyon.2024.e27757.

## References

[1] S. Peng, et al., Multiplexed microRNA detection using metal-organic framework for signal Output, ACS Appl. Bio Mater. 3 (5) (May 18, 2020) 2604–2609, https://doi.org/10.1021/acsabm.9b01189. American Chemical Society.
[2] K. Shahsavar, E. Shokri, M. Hosseini, Sensitive colorimetric detection of miRNA-155 via G-quadruplex DNAzyme decorated spherical nucleic acid, Microchim. Acta 189 (9) (2022) 357, https://doi.org/10.1007/s00604-022-05455-7.
[3] Y.-S. Borghei, M. Hosseini, M.R. Ganjali, S. Hosseinkhani, Label-free fluorescent detection of microRNA-155 based on synthesis of hairpin DNA-templated copper nanoclusters by etching (top-down approach), Sensors Actuators B Chem 248 (2017) 133–139, https://doi.org/10.1016/j.snb.2017.03.148.
[4] K. Otmani, P. Lewalle, Tumor Suppressor miRNA in cancer cells and the tumor microenvironment: mechanism of deregulation and clinical implications, Front. Oncol. 11 (October) (2021) 1–15, https://doi.org/10.3389/fonc.2021.708765.
[5] E. Ban, H. Kwon, H.S. Seo, Y.S. Yoo, E.J. Song, Screening of miRNAs in plasma as a diagnostic biomarker for cardiac disease based on optimization of extraction and qRT-PCR condition assay through amplification efficiency, BMC Biotechnol. 21 (1) (2021) 1–10, https://doi.org/10.1186/s12896-021-00710-w.
[6] N. Nagpal, R. Kulshreshtha, miR-191: an emerging player in disease biology, Front. Genet. 5 (APR) (2014), https://doi.org/10.3389/fgene.2014.00099.
[7] R. Garzon, et al., MicroRNA signatures associated with cytogenetics and prognosis in acute myeloid leukemia, Blood 111 (6) (2008) 3183–3189, https://doi.org/10.1182/blood-2007-07-098749.
[8] M.V. Iorio, et al., MicroRNA gene expression deregulation in human breast cancer, Cancer Res. 65 (16) (2005) 7065–7070, https://doi.org/10.1158/0008-5472.CAN-05-1783.
[9] M. Fassan, et al., MicroRNA expression profiling of male breast cancer, Breast Cancer Res. 11 (4) (2009) 1–10, https://doi.org/10.1186/bcr2348.
[10] K.R.M. Leite, et al., MicroRNA-100 expression is independently related to biochemical recurrence of prostate cancer, J. Urol. 185 (3) (2011) 1118–1122, https://doi.org/10.1016/j.juro.2010.10.035.
[11] A. Routhier, et al., Pharmacological inhibition of Rho-kinase signaling with Y-27632 blocks melanoma tumor growth, Oncol. Rep. 23 (3) (2010) 861–867, https://doi.org/10.3892/or.
[12] S.K. Patnaik, E. Kannisto, S. Yendamuri, Overexpression of microRNA miR-30a or miR-191 in A549 lung cancer or BEAS-2B normal lung cell lines does not alter phenotype, PLoS One 5 (2) (2010) 1–6, https://doi.org/10.1371/journal.pone.0009219.

[13] H. Luo, et al., Serum-Derived microRNAs as prognostic biomarkers in osteosarcoma: a meta-analysis, Front. Genet. 11 (August) (2020) 1–10, https://doi.org/10.3389/fgene.2020.00789.
[14] A. Zampetaki, et al., Plasma MicroRNA profiling reveals loss of endothelial MiR-126 and other MicroRNAs in type 2 diabetes, Circ. Res. 107 (6) (2010) 810–817, https://doi.org/10.1161/CIRCRESAHA.110.226357.
[15] J. Chen, Y. Qi, C.F. Liu, J.M. Lu, J. Shi, Y. Shi, MicroRNA expression data analysis to identify key miRNAs associated with Alzheimer's disease, J. Gene Med. 20 (6) (2018), https://doi.org/10.1002/jgm.3014.
[16] Y. Luo, et al., Increased serum and urinary MicroRNAs in children with idiopathic nephrotic syndrome, Clin. Chem. 59 (4) (2013) 658–666, https://doi.org/10.1373/clinchem.2012.195297.
[17] M. Hosseini, E. Ahmadi, Y.-S. Borghei, M. Reza Ganjali, A new fluorescence turn-on nanobiosensor for the detection of micro-RNA-21 based on a DNA-gold nanocluster, Methods Appl. Fluoresc. 5 (1) (Mar. 2017) 15005, https://doi.org/10.1088/2050-6120/aa5e57.
[18] K. Ma, H. Wang, H. Li, B. Xu, W. Tian, Label-free detection for SNP using AIE probes and carbon nanotubes, Sens. Actuators, B 253 (2017) 92–96, https://doi.org/10.1016/j.snb.2017.06.055.
[19] X. Ou, et al., Simultaneous detection of telomerase and miRNA with graphene oxide-based fluorescent aptasensor in living cells and tissue samples, Biosens. Bioelectron. 124 (125) (2019) 199–204, https://doi.org/10.1016/j.bios.2018.10.009.
[20] J. Haider, et al., "A Review of Synthesis, Fabrication, and Emerging Biomedical Applications of Metal-Organic Frameworks," Biomaterials Advances, vol. 140, Elsevier Ltd, Sep. 01, 2022, https://doi.org/10.1016/j.bioadv.2022.213049.
[21] Q. Zhang, C.F. Wang, Y.K. Lv, Luminescent switch sensors for the detection of biomolecules based on metal-organic frameworks, Analyst 143 (18) (2018) 4221–4229, https://doi.org/10.1039/c8an00816g.
[22] G. Férey, Hybrid porous solids: past, present, future, Chem. Soc. Rev. 37 (1) (2008) 191–214, https://doi.org/10.1039/b618320b.
[23] V.F. Cheong, P.Y. Moh, Recent advancement in metal–organic framework: synthesis, activation, functionalisation, and bulk production, Mater. Sci. Technol. 34 (9) (2018) 1025–1045, https://doi.org/10.1080/02670836.2018.1468653.
[24] C.G. Carson, A.J. Brown, D.S. Sholl, S. Nair, Sonochemical synthesis and characterization of submicrometer crystals of the metal-organic framework Cu[(hfipbb)(H2hfipbb)0.5], Cryst. Growth Des. 11 (10) (2011) 4505–4510, https://doi.org/10.1021/cg200728b.
[25] J. Gilnezhad, A. Firoozbakhtian, M. Hosseini, S. Adel, G. Xu, M.R. Ganjali, An enzyme-free Ti3C2/Ni/Sm-LDH-based screen-printed-electrode for real-time sweat detection of glucose, Anal. Chim. Acta 1250 (2023) 340981, https://doi.org/10.1016/j.aca.2023.340981.
[26] A. Firoozbakhtian, M. Hosseini, Y. Guan, G. Xu, Boosting electrochemiluminescence immunoassay sensitivity via Co–Pt nanoparticles within a Ti3C2 MXene-modified single electrode electrochemical system on raspberry pi, Anal. Chem. 95 (40) (Oct. 2023) 15110–15117, https://doi.org/10.1021/acs.analchem.3c03285.
[27] K. Shahsavar, E. Shokri, M. Hosseini, A fluorescence-readout method for miRNA-155 detection with double-hairpin molecular beacon based on quadruplex DNA structure, Microchem. J. 158 (2020) 105277, https://doi.org/10.1016/j.microc.2020.105277.
[28] D.I. Osman, et al., Nucleic acids biosensors based on metal-organic framework (MOF): paving the way to clinical laboratory diagnosis, Biosens. Bioelectron. 141 (2019), https://doi.org/10.1016/j.bios.2019.111451.
[29] Y.-S. Borghei, M. Hosseini, M.R. Ganjali, Fluorescence based turn-on strategy for determination of microRNA-155 using DNA-templated copper nanoclusters, Microchim. Acta 184 (8) (2017) 2671–2677, https://doi.org/10.1007/s00604-017-2272-6.
[30] Y.S. Borghei, M. Hosseini, M.R. Ganjali, H. Ju, Colorimetric and energy transfer based fluorometric turn-on method for determination of microRNA using silver nanoclusters and gold nanoparticles, Microchim. Acta 185 (6) (2018) 1–9, https://doi.org/10.1007/s00604-018-2825-3.
[31] W. Shi, et al., Nano-octahedral bimetallic Fe/Eu-MOF preparation and dual model sensing of serum alkaline phosphatase (ALP) based on its peroxidase-like property and fluorescence, Mater. Sci. Eng. C 129 (Oct) (2021), https://doi.org/10.1016/j.msec.2021.112404.
[32] S.S.M. Ameen, I.B. Qader, H.A. Qader, F.K. Algethami, B.Y. Abdulkhair, K.M. Omer, Dual-state dual emission from precise chemically engineered bi-ligand MOF free from encapsulation and functionalization with self-calibration model for visual detection, Microchim. Acta 191 (1) (2024) 1–9, https://doi.org/10.1007/s00604-023-06148-5.
[33] M. Hu, et al., CoNi bimetallic metal–organic framework as an efficient biosensing platform for miRNA 126 detection, Appl. Surf. Sci. 542 (November 2020) (2021) 148586, https://doi.org/10.1016/j.apsusc.2020.148586.
[34] S.S. Mohammed Ameen, F.O. Qasim, H.S. Alhasan, K.H. Hama Aziz, K.M. Omer, Intrinsic dual-state emission zinc-based MOF rodlike nanostructures with applications in smartphone readout visual-based detection for tetracycline: MOF-based color tonality, ACS Appl. Mater. Interfaces 15 (39) (2023) 46098–46107, https://doi.org/10.1021/acsami.3c11950.
[35] G.K. Ali, K.M. Omer, Nanozyme and stimulated fluorescent Cu-based metal-organic frameworks (Cu-MOFs) functionalized with engineered aptamers as a molecular recognition element for thrombin detection in the plasma of COVID-19 patients, ACS Omega 7 (41) (2022) 36804–36810, https://doi.org/10.1021/acsomega.2c05232.
[36] H.M. Meng, Z. Li, X. Shi, X. Geng, L. Qu, DNAzyme−metal−organic framework two-photon nanoprobe for in situ monitoring of apoptosis-associated Zn2+ in living cells and tissues, ACS Sens. 5 (10) (2020) 3150–3157, https://doi.org/10.1021/acssensors.0c01271.
[37] K. Yu, T. Wei, Z. Li, J. Li, Z. Wang, Z. Dai, Construction of molecular sensing and logic systems based on site-occupying effect-modulated MOF-DNA interaction, J. Am. Chem. Soc. 142 (51) (Dec. 2020) 21267–21271, https://doi.org/10.1021/jacs.0c10442.
[38] H. Furukawa, K.E. Cordova, M. O'Keeffe, O.M. Yaghi, The chemistry and applications of metal-organic frameworks, Science 341 (6149) (2013), https://doi.org/10.1126/science.1230444.
[39] S. Peng, et al., Metal-organic frameworks for precise inclusion of single-stranded DNA and transfection in immune cells, Nat. Commun. 9 (1) (2018) 1–10, https://doi.org/10.1038/s41467-018-03650-w.
[40] Y. peng Huo, S. Liu, Z. xian Gao, B. an Ning, Y. Wang, State-of-the-art progress of switch fluorescence biosensors based on metal-organic frameworks and nucleic acids, Microchim. Acta 188 (5) (2021) 1–29, https://doi.org/10.1007/s00604-021-04827-9.
[41] E. Mirsadoughi, A.B. Pebdeni, M. Hosseini, Sensitive colorimetric aptasensor based on peroxidase-like activity of ZrPr-MOF to detect Salmonella Typhimurium in water and milk, Food Control 146 (Apr. 2023), https://doi.org/10.1016/j.foodcont.2022.109500.
[42] H. Abdolmohammad-Zadeh, F. Ahmadian, A fluorescent biosensor based on graphene quantum dots/zirconium-based metal-organic framework nanocomposite as a peroxidase mimic for cholesterol monitoring in human serum, Microchem. J. 164 (January) (2021) 106001, https://doi.org/10.1016/j.microc.2021.106001.
[43] S.M. Sheta, S.M. El-Sheikh, M.M. Abd-Elzaher, A novel optical approach for determination of prolactin based on Pr-MOF nanofibers, Anal. Bioanal. Chem. 411 (7) (2019) 1339–1349, https://doi.org/10.1007/s00216-018-01564-6.
[44] H.-Q. Yin, X.-Y. Wang, X.-B. Yin, Rotation restricted emission and antenna effect in single metal–organic frameworks, J. Am. Chem. Soc. 141 (38) (Sep. 2019) 15166–15173, https://doi.org/10.1021/jacs.9b06755.
[45] X. Wen, C. Li, Z. Zhou, Y. He, J. He, X. Hou, Wavelength-shift-based visual fluorescence sensing of aspartic acids using Eu/Gd-MOF through pH triggering, Talanta 265 (April) (2023) 124778, https://doi.org/10.1016/j.talanta.2023.124778.
[46] S.S. Mohammed Ameen, N.M. Sher Mohammed, K.M. Omer, Ultra-small highly fluorescent zinc-based metal organic framework nanodots for ratiometric visual sensing of tetracycline based on aggregation induced emission, Talanta 254 (October 2022) 2023, https://doi.org/10.1016/j.talanta.2022.124178.
[47] X. Wang, et al., A MOF/DNA luminescent sensing platform for detection of potential COVID-19 biomarkers and drugs, Chem. Sci. 14 (20) (2023) 5386–5395, https://doi.org/10.1039/D3SC00106G.
[48] L. Wang, Z. Hu, S. Wu, J. Pan, X. Xu, X. Niu, A peroxidase-mimicking Zr-based MOF colorimetric sensing array to quantify and discriminate phosphorylated proteins, Anal. Chim. Acta 1121 (Jul. 2020) 26–34, https://doi.org/10.1016/j.aca.2020.04.073.
[49] H.S. Wang, et al., Insight into the unique fluorescence quenching property of metal-organic frameworks upon DNA binding, Anal. Chem. 89 (21) (Nov. 2017) 11366–11371, https://doi.org/10.1021/acs.analchem.7b02256.

[50] L. Liu, S. Zhu, Y. Wei, X.L. Liu, S. Jiao, J. Yang, Ultrasensitive detection of miRNA-155 based on controlled fabrication of AuNPs@MoS2 nanostructures by atomic layer deposition, Biosens. Bioelectron. 144 (August) (2019) 111660, https://doi.org/10.1016/j.bios.2019.111660.
[51] Y. Wu, J. Han, P. Xue, R. Xu, Y. Kang, Nano metal-organic framework (NMOF)-based strategies for multiplexed microRNA detection in solution and living cancer cells, Nanoscale 7 (5) (2015) 1753–1759, https://doi.org/10.1039/c4nr05447d.
[52] J. Tang, et al., Biocatalysis-mediated MOF-to-prussian blue transformation enabling sensitive detection of NSCLC-associated miRNAs with dual-readout signals, Biosens. Bioelectron. 206 (2022), https://doi.org/10.1016/j.bios.2022.114139.
[53] H. Shao, J. Lu, Q. Zhang, Y. Hu, S. Wang, Z. Guo, Ruthenium-based metal organic framework (Ru-MOF)-derived novel Faraday-cage electrochemiluminescence biosensor for ultrasensitive detection of miRNA-141, Sensors Actuators B Chem 268 (2018) 39–46, https://doi.org/10.1016/j.snb.2018.04.088.
[54] G.-H. Qiu, et al., A metal-organic framework based PCR-free biosensor for the detection of gastric cancer associated microRNAs, J. Inorg. Biochem. 177 (2017) 138–142, https://doi.org/10.1016/j.jinorgbio.2017.08.036.